Scientia Iranica A (2011) 18 (6), 1198–1206

Sharif University of Technology

Scientia Iranica

Transactions A: Civil Engineering

www.sciencedirect.com

A field study of the behavior of small-scale single rammed aggregate piers, testing methodology and interpretation

H.R. Razeghi *, **B. Niroumand**, **H. Ghiassian**

School of Civil Engineering, Iran University of Science and Technology, Narmak, Tehran, P.O. Box 16765-163, Iran

Received 30 January 2011; accepted 31 October 2011

KEYWORDS

Rammed aggregate piers;
Pier stiffness;
Soil reinforcement;
Slenderness ratio;
Load tests;
Design limit loads.

Abstract This paper presents the measured behavior of small-scale single rammed aggregate piers as a function of the piers' slenderness ratio. For this purpose, loading tests at the site were carried out on two groups of single rammed aggregate piers with a constant diameter of 135 mm and variable lengths of 350–1000 mm, and two groups with a constant length of 1000 mm and various diameters of 105–185 mm. The testing area consisted of relatively uniform saturated soft alluvial clay overlain by a 1-m-thick wet soft-to-stiff silt layer. Results show that when length and diameter change, the pier load and top settlement variations at the design limit, in terms of the slenderness ratio, are not in the same direction while other design limit parameters' variations are. The variations of design limit parameters in the two modes of change to pier length and diameter including the applied load, top settlement, stiffness modulus and pier modulus, in terms of the slenderness ratio, make a linear function while the variations of load and settlement ratio show an exponential function. Interpretations of the test results are particularly focused on the load-settlement behavior and variations of design limit parameters as a function of pier slenderness ratios.

1. Introduction

Rammed Aggregate Piers (RAPs) are one of the soft soils reinforcement techniques that in recent years have been increasingly used to reduce intolerable settlements, as well as to improve the bearing capacity and stiffness in various building and transportation projects [1–5]. The construction process of rammed aggregate piers consists of three steps: cavity drilling, making end-resistant bulbs, and implementing pier shafts. End-resistant bulbs and pier shafts are constructed using layers of open graded and well graded gravel, respectively [1,6,7]. The nominal thickness of aggregate layers, which has been documented in the literature by a number of authors, is 0.3 m, and each layer is compacted using a specially designed beveled tamper connected to a hydraulic hammer [8,9].

The hydraulic hammer delivers between 1 and 2 million ft-lbs of energy to the RAP at approximately 400 blows per minute [7]. As a result of aggregate compaction, the soft soil at the end bulb deforms downwards and laterally, and in the next aggregate layers, the soft soil around the pier deforms laterally under compression. An increase in the pier diameter due to the compaction of aggregate layers helps the matrix soil around the pier to be compacted and the pier stiffness to increase [10–13]. Unlike drilled deep and shallow foundation systems, parameter values for rammed aggregate piers are derived from the results of modulus tests carried out at each project site [14]. Predicting the load–settlement and load transfer behaviors is important in the designing of RAPs [15]. The designing of this system and developing of analytical methods involving RAPs require a full understanding of the variations of design limit parameters as a function of pier slenderness ratios. Changes to the pier slenderness ratio can be a function of changes to the pier length or diameter. Therefore, two groups of single RAPs with different lengths and diameters and various slenderness ratios ranging between 2.6 and 9.5 were constructed and tested in the soft soils of the Bushehr Special Economic Zone in south Iran. Soil properties and layer conditions at the test site were evaluated by means of conventional laboratory and in situ tests. The applied load on the top, and top and tip settlements of

* Corresponding author.
E-mail address: razeghi@iust.ac.ir (H.R. Razeghi).

1026-3098 © 2012 Sharif University of Technology. Production and hosting by Elsevier B.V. Open access under CC BY-NC-ND license.
Peer review under responsibility of Sharif University of Technology.

doi:10.1016/j.scient.2011.11.016

Production and hosting by Elsevier

the piers, were measured. The piers tip load is determined by the measured pier tip settlement and by using the load–settlement curve of end-resistant bulbs, which is obtained directly from the loading tests on the end-resistance bulbs. In this paper, the process of construction and the testing method of small-scale RAPs', as well as the method of measuring their load–settlement data at the site, are presented. Furthermore, the load–settlement behavior, tip to top load ratio and stiffness modulus of RAPs are compared in terms of the slenderness ratio in the two modes of variable pier length and variable pier diameter. Also, variations in the RAP design limit parameters as a function of pier slenderness ratio have been studied.

2. Construction and loading of single RAPs

In this study, two groups of single RAP were tested. In the first group, five cavities with end-resistant bulbs and five single RAPs with a constant diameter of 135 mm and variable lengths of 350, 550, 700, 850 and 1000 mm were constructed. The second group consisted of four cavities with end-resistant bulbs, and four single RAPs with a constant length of 1000 mm and variable diameters of 105, 135, 155 and 185 mm. The RAP with the length of 1000 mm and diameter of 135 mm was shared by both groups. Based on the influence radius (r_m) presented by Randolph and Wroth [16], the distance between the RAPs was arranged in such a way that the RAPs could not affect each other. The influence radius is the distance at which the shear stress effect becomes negligible and can be computed by the following equation [15,16]:

$$r_m = 2.5(1 - \upsilon)L, \tag{1}$$

where υ sand L are the soil Poisson ratio and RAP length, respectively. The RAP shafts were constructed using successively compacted layers of crushed lime stone classified as GW ($C_u = 9.63$, $C_c = 1.83$ and $D_{10} = 1.08$ mm), which was made up of %69 gravel ($D_{\max} = 22$ mm), %29.2 sand and %1.8 silt in weight. On the other hand, the end-resistant bulbs were constructed using layers of open graded gravel with a maximum size of 22 mm. The thickness and compaction duration of each layer were 100 mm and 10 s, respectively. The weight of the electric rammer and its accessories, the impact rate and the impact energy were 105 lb, 1030 rpm and 60 J, respectively. The impacts were applied to each layer by a beveled tamper connected to an electric rammer. The thickness of the circular steel beveled tamper was between 25 and 45 mm and its diameter was about 20 mm less than the diameter of each cavity. Figure 1 depicts the electric rammer, special tampers and a constructed RAP after the loading test.

In order to load the rammed aggregate piers, mobile reaction beams, in the form of a loading cart and a modular rail system, were used, both to speed up the tests and to make them more economical. The advantage of this system was in the provision of a mobile support which could bear the applied reaction force of the loading jack. In this system, four rails with a 6 m length were used. These rails were moved in proportion to the forward movement of the loaded cart. Each rail was connected to six 1 m-long wooden pads with a 150 × 150 mm cross section.

This system was designed to support a maximum force of 100 kN applied by the jack at the center of the cart. In order to prepare the cart path, two longitudinal strips of 50 m length, 2.6 m width and 0.4 m depth were excavated in the soft ground and the spoils were disposed. Then, the excavation area was filled up with rubble. The filling was carried out manually without disturbing the bed area of the ground between the strips. At the next stage, two 0.3 m-thick sub-base layers of soil

Figure 1: Illustrations of (a) electric rammer, (b) special tampers by 45 degree bezel, and (c) a typical of RAPs after loading.

were watered and compacted with a roller on the stone layer. Figure 2 shows the measurement details of the loading cart and the modular rail system on the compacted fill.

In order to apply a compressive force to the piers, a jack with a maximum load capacity of 300 kN and 100 mm stroke was used. To measure the applied force on the piers, a load cell of 100 kN capacity (with a 5 N accuracy and a digital indicator) was utilized between the jack piston and the loading cart. The jack load was transferred to the top of the piers using a steel shaft connected to a loading plate. The diameter of the steel shaft and the thickness of the loading plate were 50 mm and 20 mm, respectively. The diameter of the loading plate was equal to the nominal diameter of the trial pier. The load transfer shaft was connected to a jack by a jack holder. In order to maintain the load axially and to prevent the jack from tilting during loading, a four-thronged shaft holder was designed and constructed. At the center of the shaft holder was a cylindrical steel of 52 mm inner diameter and 200 mm length. By passing the load transfer shaft through the cylindrical steel, the shaft was not allowed to tilt during loading. In practice, after establishing the loading plate on top of the pier and connecting the shaft to it, the shaft holder was beaten and leveled into the ground. The loading system was designed so that there was not any possibility of the loading plate tilting during the loading test. Therefore, the vertical deflection was measured with a dial gauge only. In order to measure the pier tip settlement, a mechanical settlement set with an accuracy of 0.01 mm was designed and built. A circular hard plastic (reference telltale plate) with a 10 mm thickness was installed between the end resistant bulb and the pier shaft. The telltale plate was connected to a mechanical settlement, set at the top of the pier with a cord that was protected by a PVC sleeve 12 mm in diameter. Figure 3 shows the elements of the RAPs loading and load–settlement measuring systems. During the loading test of each RAP, the applied load on top of the pier (P_t), top settlement (δ_t) and tip settlement (δ_b) were measured at specified times. The piers tip load was determined by the measured pier tip settlement and

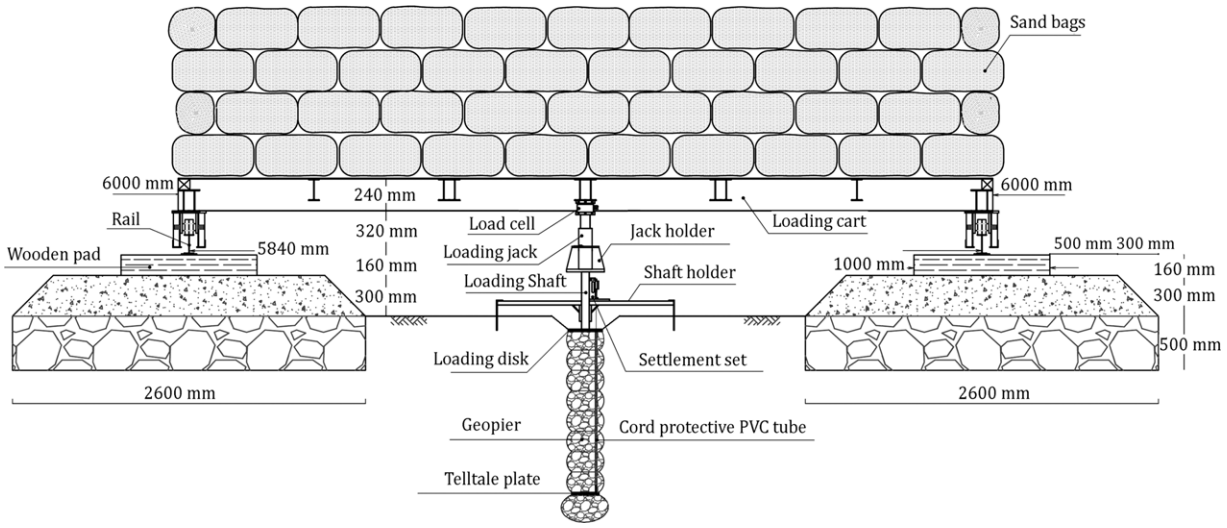

Figure 2: Measurements of loading cart and modular rails system on compacted fill.

using the load–settlement curve of the end-resistant bulb. This curve was obtained directly from loading the end-resistance bulb in the same condition as the pier end-resistance bulb.

3. Site investigation

Various in situ and laboratory tests were carried out to identify the geotechnical condition of the test site and determine soil stratification and soil physical and mechanical parameters for bearing capacity and settlement computations. The results show that in the range of 4 m deep, there were three soil layers including a thin 1 m thick layer of moist brown silt (ML), a yellow 1.4 m thick layer of soft clay (CL) and a 1.6 m thick gray layer of soft clay (CL) in uniform condition. In situ tests included Standard Penetration Tests (SPT) and Plate Load Tests (PLT). The laboratory tests conducted in this study included unit weight, soil classification, water content, one-dimensional consolidation, uniaxial compression tests and direct shear tests. Figure 4 shows the profiles of natural moisture content, Atterberg's limits and N-blows of SPT. A summary of the engineering properties of the soil layers is presented in Table 1.

4. Modulus load test results

The load tests of rammed aggregate piers were carried out according to the ASTM D-1143 standard (used for pile load tests) with stress control. In this study, the load tests were continued until the settlement of the pier top reached 25.4 mm. After performing the load test on RAPs and recording the values of the applied load at the pier top (P_t), top settlement (δ_t) and tip settlement (δ_b), the curves of P_t–δ_t and P_t–δ_b were drawn in a Cartesian coordinate system for each pier. The purpose of these curves in a common system is to determine the design limit load and identify the governing behavior of the RAPs.

Usually, the initial and final part of the P_t–δ_t curve is linear [14]. The design limit load of a RAP corresponds to the point on the P_t–δ_t curve with maximum curvature (or minimum radius of curvature). The point of maximum curvature is determined by the intersection of the two legs of the bi-linear P_t–δ_t curve. For drawing the q_t–δ_t and q_t–δ_b curves, the applied stress (q_t) can be calculated by dividing the applied load (P_t) by the pier cross section (A_P). Figure 5 shows the applied stress-settlement behavior at the top of the RAPs in two modes: (a) bulging deformation and (b) tip deformation. According to Figure 5(a), the lack of curvature at the q_t–δ_b curve after the inflection stress represents the occurrence of bulging deformation at the top of the pier. Also, the tip deformation is identified by observation of the curvature at the q_t–δ_b curve after the inflection stress (see Figure 5(b)). Wissmann et al. [17] provide a summary of 31 load tests performed on rammed aggregate piers installed in silty and clayey soils (ML, CL and SM) [17]. The results indicate that rammed aggregate piers with slenderness ratios (i.e., length to diameter ratio) greater than 3.5 are more likely to deform in bulging whereas tip deformation is more likely to occur with smaller slenderness ratios [15]. In fact, as the pier slenderness ratio increases, the load portion of pier shaft skin becomes more than the load transferred at the bottom of the pier. In this case when the applied load at the top of the pier is increased, pier settlement will be caused by bulging deformation.

4.1. Load–settlement results

Figure 6 shows the measured load–settlement including P_t–δ_t and P_t–δ_b curves of the two groups of single RAPs. As shown, the governing deformation in all piers with a constant diameter of 135 mm and slenderness ratios between 2.6 and 7.4 is tip deformation. Furthermore, in piers with a constant length of 1000 mm and slenderness ratios between 5.4 and 9.5, the governing deformation in the pier with the slenderness ratio of 9.5 (and diameter of 105 mm) is bulging deformation. In other piers with slenderness ratios between 5.4 and 7.4, tip deformation governs. In total, the governing deformation in RAPs with slenderness ratios between 2.6 and 7.4 is tip deformation and, in the RAP with the slenderness ratio of 9.5, it is bulging deformation. According to the results presented by Wissmann et al. [17], RAPs with slenderness ratios smaller than 3.5 are more likely to experience tip-settlement, whereas in this study, RAPs with slenderness ratios smaller than 7.4 have such a tendency. This difference can be caused by the lack of uniformity of the ML layer and the higher stiffness of the upper part as opposed to the lower part of the layer.

4.2. Load ratio (tip to top)

Figure 7 shows a comparison of the curves of the load ratio (P_b/P_t) as a function of the applied stress (q_t) at the top of

Table 1: Summary of physical and mechanical properties of soil layers.

Layer number	USCS classification	Depth limits (m)	Soil properties					
			γ_{wet} (kN/m^3)	ω (%)	C' (kPa)	φ' (°)	C_u (kPa)	Es (kPa)
1	Silt layer (ML)	0.15–1.15	17–18.9	27–31	1–2[a]	25[a]	18–75[b]	5400–6600[c]
2	Clay layer (CL)	1.15–2.55	16.4	43	5	19.7	7	3300
3	Clay layer (CL)	2.55–4.15	18.3	37	5	23	14	3300

[a] Consolidated—drained direct shear tests.
[b] Uniaxial compression tests.
[c] From standard penetration tests.

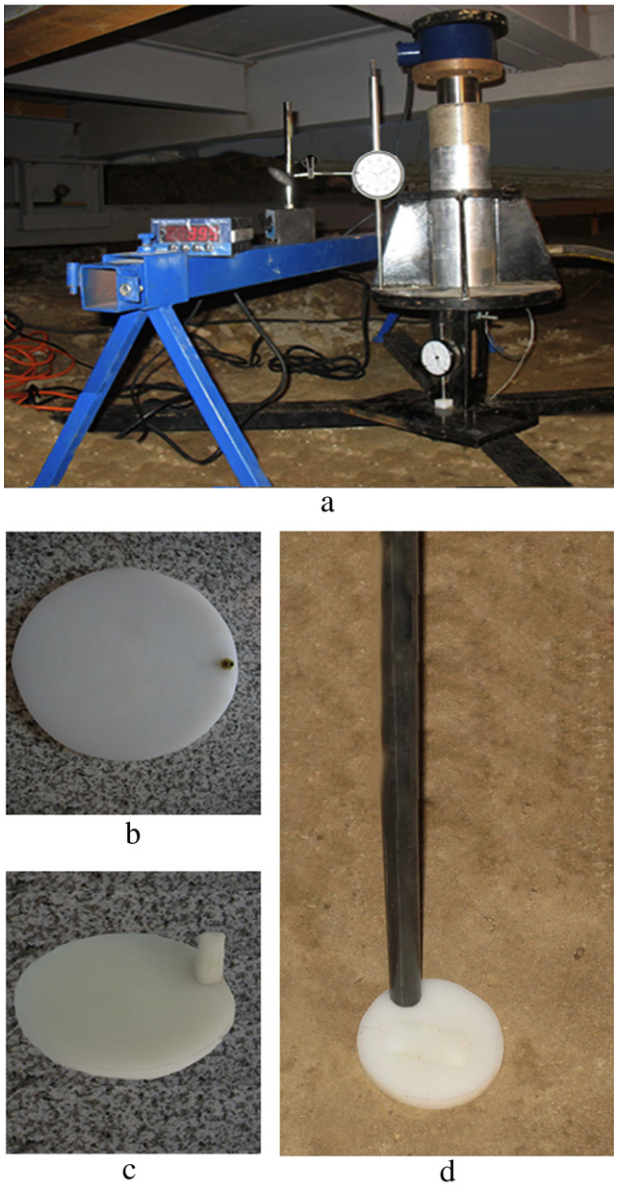

Figure 3: Illustrations of (a) the elements of RAPs loading system in place, (b) reference telltale plate made of hard plastic, (c) PVC cord protective tube holder connected to reference telltale plate, and (d) elements of the settlement set before installing into the cavity.

the RAPs in the two trial groups with a constant diameter of 135 mm and lengths between 350 and 1000 mm, and with a constant length of 1000 mm and different diameters of 105–185 mm. As shown, as the applied stress at the pier top increases, the load ratio (tip to top) is also increased. However, the rates of increase of the load ratio in the piers of these two

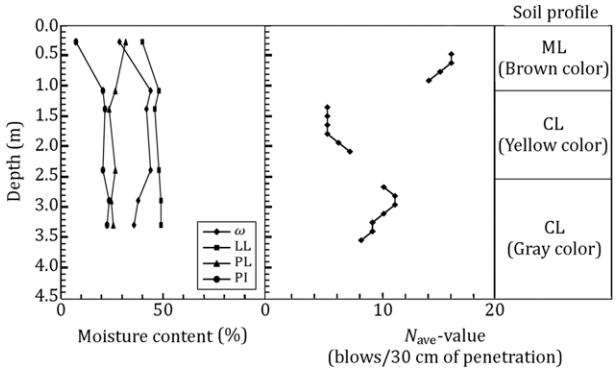

Figure 4: Summary of results and profiles of (a) moisture content and Atterberg limits, and (b) N_{avg}-blows SPT.

groups are different. In the group with the constant length of 1000 mm, the rate of increase of the load ratio in piers with diameters of 135, 155 and 185 mm is considerably higher than the rate of increase of the load ratio in the pier with the diameter of 105 mm. In addition, by increasing the applied stress at the top of the pier, the difference is also raised. The load ratio (tip to top) in the pier with the diameter of 105 mm is in the range of 2%–5%, and in piers with diameters of 135, 155 and 185 mm in the range of 1%–19%. In RAPs with a constant diameter of 135 mm, by increasing pier length, the load ratio (tip to top) is decreased, and for lengths longer than 850 mm, the variation in load ratio is very little. The load ratio in piers with lengths of 350, 550 and 700 mm is in the range of 25%–36%, 17%–23% and 12%–22%, and in the piers with lengths of 850 and 1000 mm, in the range of 6%–15%, on average.

4.3. Pier stiffness

For determining the RAPs stiffness modulus, a steel plate was used with a diameter equal to the nominal diameter of the piers. Figure 8 shows a comparison of the curves of the pier stiffness modulus (K_{SP}) as a function of the applied stress at the top of the RAPs in two trial groups with different lengths and diameters. As shown, when the applied stress increases, the pier stiffness modulus decreases. Also, with constant applied stress, increasing pier length leads to an increase in the pier stiffness modulus, and an increase in pier diameter causes a decrease in the pier stiffness modulus. The stiffness modulus in the pier with a diameter of 105 mm is constant at 1330 kPa in compressive stress while in the other piers, the stiffness modulus is descending.

5. Design limit results

5.1. Design limit load and inflection stress

Figure 9 shows the variation of the design limit load (P_d) as a function of the slenderness ratio of the RAPs in two trial

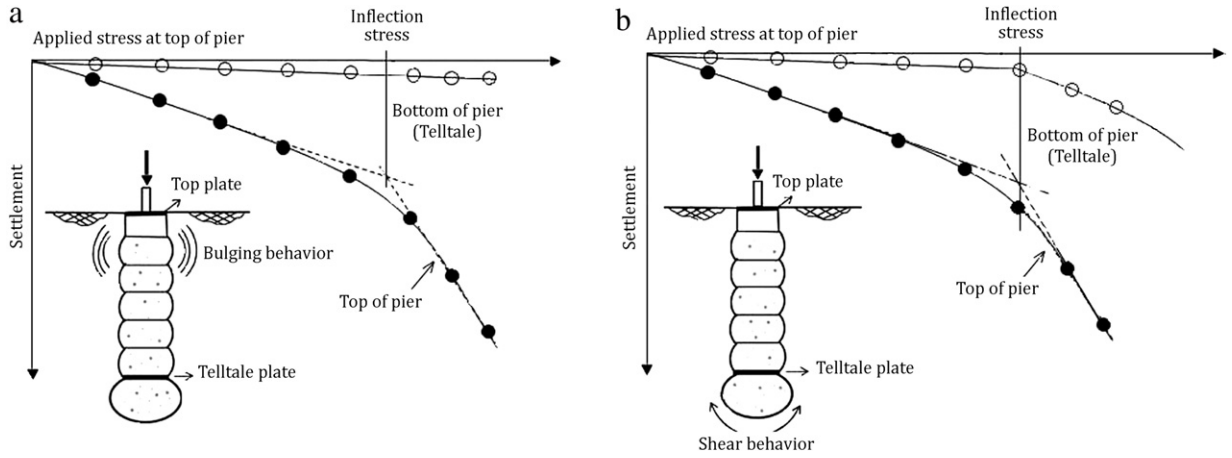

Figure 5: Modulus test results and determination of inflection stress for (a) bulging behavior at the top of pier, and (b) tip-deformation behavior at the bottom of pier.

groups with a constant diameter of 135 mm and slenderness ratios of 2.6, 4, 5.2, 6.3 and 7.4, and with a constant length of 1000 mm and slenderness ratios of 5.4, 6.5, 7.4 and 9.5. For piers with a constant diameter of 135 mm and lengths of 350, 550, 700, 850 and 1000 mm, the design limit loads are 13.65, 14.65, 17.75, 19.45 and 21.75 kN, respectively. For piers with a constant length of 1000 mm and diameters of 105, 135, 155 and 185 mm, the design limit loads are 13.85, 21.75, 24.85 and 27.75 kN, respectively.

As shown, for piers with a constant diameter and different lengths, the design limit load has an ascending trend when increasing the slenderness ratio, and for piers with a constant length and different diameters, a descending trend. Therefore, as can be seen, the trends of variation of the design limit load as a function of slenderness ratios in the two modes of variable diameters and variable lengths are not in the same direction. Figure 10 shows the variations of the inflection stress (q_d) as a function of the slenderness ratio of the RAPs in the trial groups. In this case, unlike in Figure 8, the inflection stress of the piers in the two groups goes up when increasing the slenderness ratio.

5.2. Load ratio (tip to top)

Figure 11 shows the variation of the tip to top load ratio at the design limit (P_b/P_t) as a function of the slenderness ratio of the RAPs in the two trial groups with different lengths and diameters. For piers with a constant diameter of 135 mm and lengths between 350 and 1000 mm, the load ratios for the slenderness ratios of 2.6, 4, 5.2, 6.3 and 7.4 are 35.9%, 24.2%, 22.1%, 11.9% and 9.8%, respectively. In these piers, when increasing the length, the slenderness ratio is increased and load ratio decreased. For piers with a constant length of 1000 mm and different diameters of 105–185 mm, the load ratios for the 9.5, 7.4, 6.5 and 5.4 slenderness ratios are 5%, 10%, 13% and 9%, respectively. In these piers, when increasing the diameter, the slenderness ratio is decreased and load ratio increased. In the pier with a diameter of 185 mm, the un-normal decrease in load ratio is probably due to a change in soil conditions. As seen in Figure 11, in each of the two groups of pier, increasing the slenderness ratio causes a descending trend in the load ratio. Between the trial piers, the minimum load ratio belongs to the pier with the diameter of 105 mm and length of 1000 mm in which bulging deformation occurred. In other piers with tip deformation, the load ratio is between 10% and 36%.

5.3. Settlement ratio (tip to top)

Figure 12 shows the variation of the tip to top settlement ratio at the design limit (δ_b/δ_t) as a function of the slenderness ratio of the RAPs in the two trial groups with different lengths and diameters. For piers with a constant diameter of 135 mm and lengths between 350 and 1000 mm, the measured settlement ratios for the 2.6, 4, 5.2, 6.3 and 7.4 slenderness ratios are 90%, 44%, 36%, 31% and 24%, respectively. In these piers, when increasing length, the slenderness ratio is increased and settlement ratio decreased. For piers with a constant length of 1000 mm and different diameters of 105–185 mm, the measured settlement ratios for the 9.5, 7.4, 6.5 and 5.4 slenderness ratios are 14%, 24%, 35% and 21%, respectively. In these piers, increasing diameter leads to a decrease in the slenderness ratio and an increase in the settlement ratio.

In piers with a diameter of 185 mm, the un-normal decrease in the settlement ratio is probably due to a change in soil conditions. As seen in Figure 12, in the two groups of pier, increasing the slenderness ratio leads to a descending trend in settlement ratio. Between the trial piers, the minimum measured settlement ratio belongs to the pier with a diameter of 105 mm and length of 1000 mm in which bulging deformation occurred. In other piers with tip deformation, the settlement ratio is between 21% and 90%.

5.4. Top settlement

Figure 13 shows the variations of the top settlement at the design limit (δ_t) as a function of the slenderness ratio of the RAPs in the two trial groups with different lengths and diameters. For piers with a constant diameter of 135 mm and lengths between 350 and 1000 mm, the variations of the top settlement at the design limit are between 9 and 10.8 mm, whereas for piers with a constant length of 1000 mm and different diameters of 105–185 mm, the variations of the top settlement at the design limit are between 7.2 and 13.1 mm. As shown, for piers with a constant diameter and variable lengths, the top settlement at the design limit reveals an ascending trend when increasing the slenderness ratio, and for piers with a constant length and variable diameters, the top settlement has a descending trend. Therefore, the trend of variations of the top settlement at the design limit as a function of the slenderness ratio in the modes of variable diameters and variable lengths are not in the same direction.

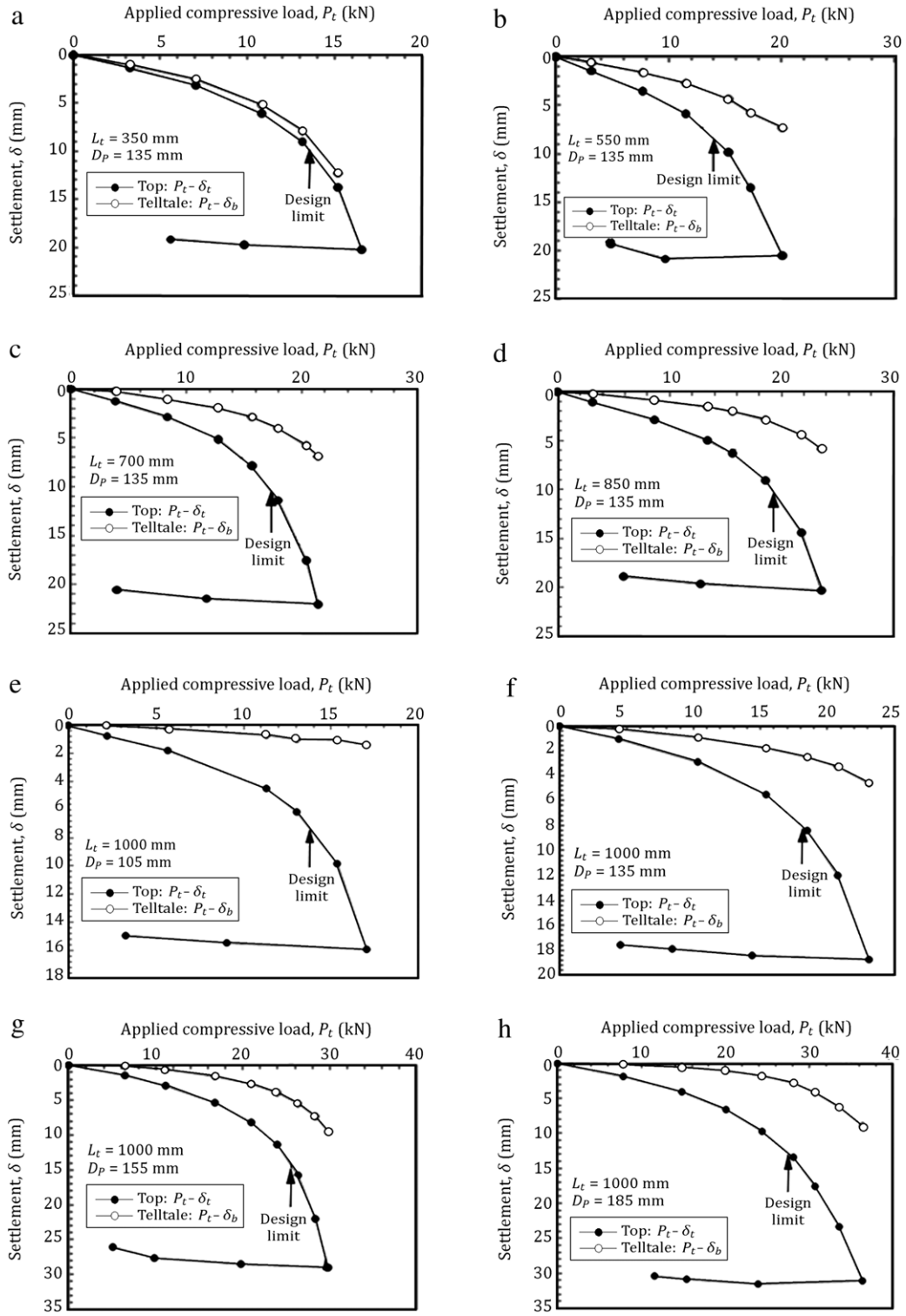

Figure 6: Measured load–settlement curves are presented for a group of single rammed aggregate piers by a constant diameter of 135 mm, and different lengths between 350 and 1000 mm, and a group with constant length of 1000 mm, and different diameters between 105 and 185 mm.

5.5. Pier elastic modulus

The average modulus of elasticity of the rammed aggregate piers can be obtained from the results of the load tests (ignoring the created stresses in the pier-soil contact matrix) using the following equation [15]:

$$E_{SP} = (P_{avg}.L_t)/(A_P.\Delta L_t), \quad (2)$$

where P_{avg} is the average of measured loads at the top (P_t) and bottom (P_b) of the pier; L_t is distance of the telltale plate to top plate; A_p is cross-sectional area of the pier; and ΔL_t is measured shortening length of the pier at each loading step.

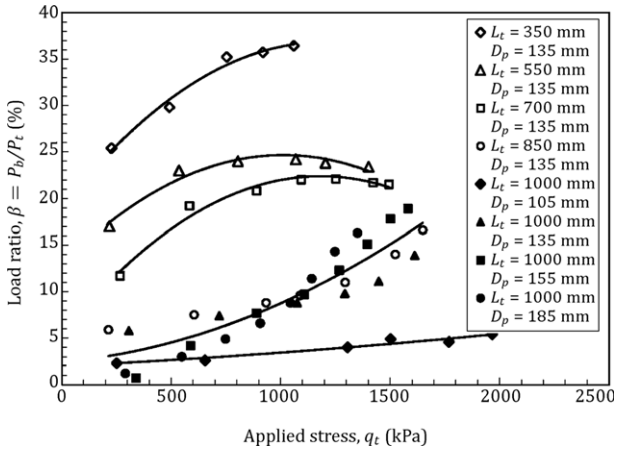

Figure 7: Comparison of the load ratio variations (tip to top) as a function of applied stress at the top of RAPs.

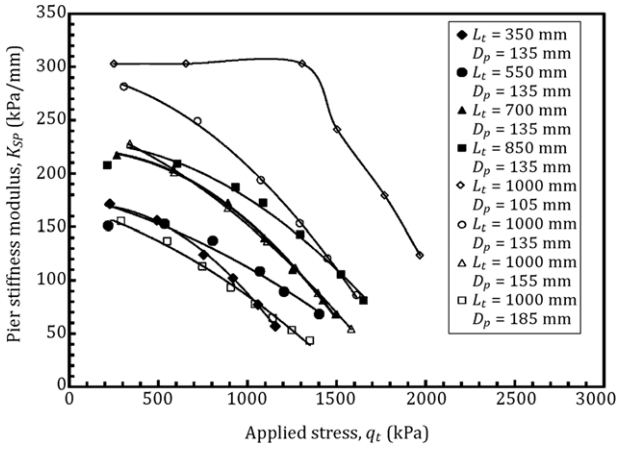

Figure 8: Comparison of the stiffness modulus variations of two groups of RAPs by different lengths and diameters as a function of applied stress at the top of the RAPs.

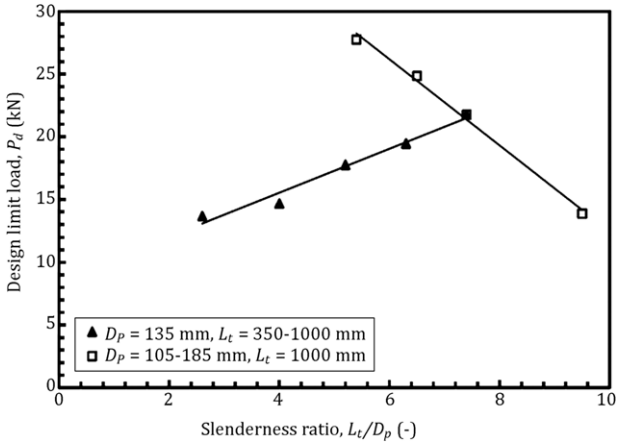

Figure 9: Comparison of the design limit load variations as a function of the slenderness ratio of RAPs.

Figure 14 shows the variation of piers elastic modulus at the design limit (E_{SP}) as a function of the slenderness ratio of the RAPs in the two trial groups with variable lengths and diameters. For piers with a constant diameter of 135 mm and lengths between 550 and 1000 mm, variations of the piers

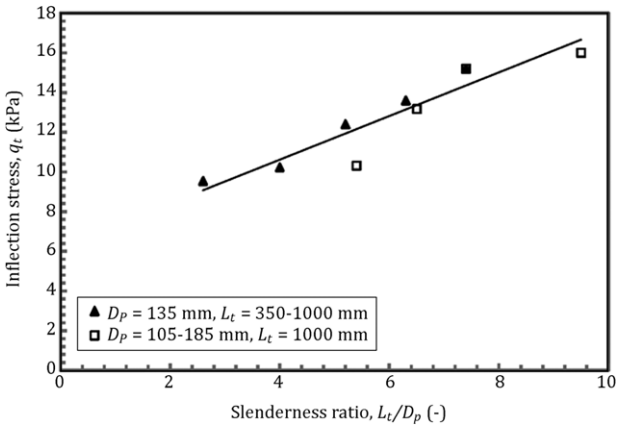

Figure 10: Comparison of inflection stress variations as a function of the slenderness ratio of RAPs.

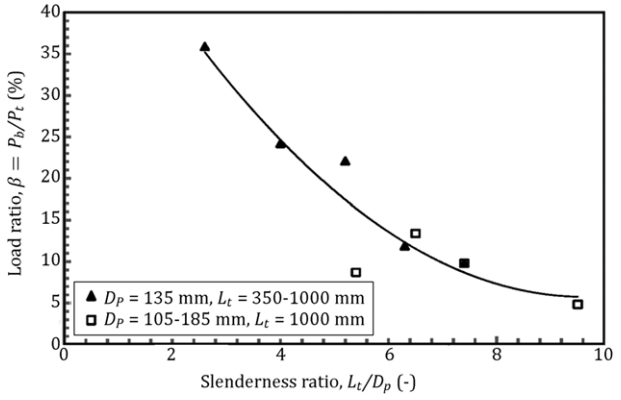

Figure 11: Comparison of the load ratio variations (tip to top) at design limit as a function of the slenderness ratio of RAPs.

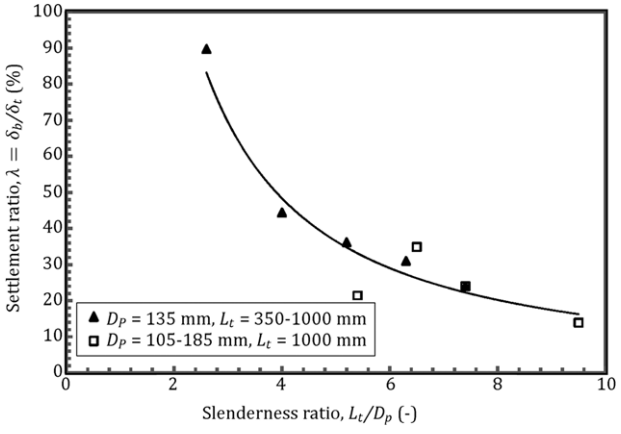

Figure 12: Comparison of the settlement ratio variations (tip to top) at design limit as a function of the slenderness ratio of RAPs.

elastic modulus at the design limit are between 70 and 125 MPa, whereas for piers with a constant length of 1000 mm and different diameters of 105–185 mm, variations of the piers elastic modulus at the design limit are between 55 and 135 MPa. As shown, when increasing the slenderness ratio (i.e. increasing the pier length and decreasing the pier diameter), pier elastic modulus shows an ascending trend.

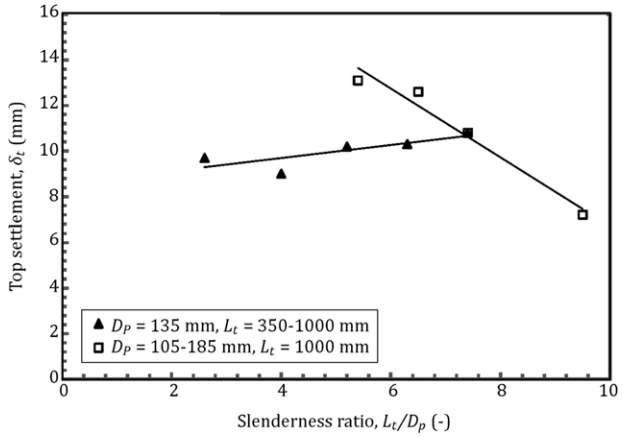

Figure 13: Comparison of top settlement variations at design limit as function of the slenderness ratio of RAPs.

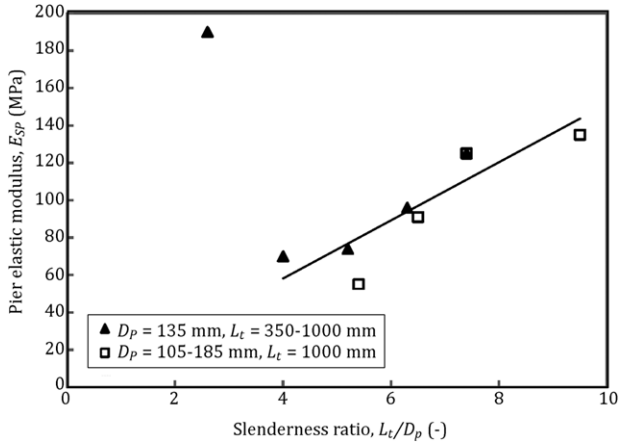

Figure 14: Comparison of the pier elastic modulus variations at design limit as a function of the slenderness ratio of RAPs.

5.6. Pier stiffness modulus

Figure 15 shows the variations of the piers stiffness modulus at the design limit (K_{SP}) as a function of the slenderness ratio of the RAPs in the two trial groups with varying lengths and diameters. For piers with a constant diameter of 135 mm and lengths between 350 and 1000 mm, variations of the piers stiffness modulus at the design limit are between 152 and 265 kPa/mm, whereas for piers with a constant length of 1000 mm and variable diameters of 105–185 mm, variations of the piers stiffness modulus at the design limit are between 146 and 347 kPa/mm. As shown, in the piers of both trial groups, increasing the slenderness ratio makes for a decrease in the pier stiffness modulus.

6. Conclusions

In this study, in order to evaluate the effect of the piers slenderness ratio (in the two modes of variable lengths and variable diameters) on the design limit parameters of RAPs, the results of eight pier modulus tests at the trial site were analyzed. The major findings of this study include the following:

- In all RAPs with slenderness ratios between 2.6 and 7.4, tip deformation occurred. However, according to the results given by Wissmann et al. [17], the RAPs with slenderness ratios greater than 3.5 are more likely to experience bulging deformation, and tip deformation is more likely to occur in lower slenderness ratios. This difference can be caused by the lack of uniformity of the ML layer, that is a higher stiffness of the upper part as opposed to lower part of the layer. The discrepancy can also be due to the difference in the scale of the RAPs construction.
- In RAPs, the load and top settlement variations at the design limit as a function of the slenderness ratio are not in the same direction when the length or diameter changes. With a change in RAP length, variations of the load and settlement at the design limit, in terms of slenderness ratio, make for a linear function. With an increase in the slenderness ratio, the variations reveal an ascending trend, whereas with a change in RAP diameter, increasing the slenderness ratio makes for a descending trend.
- When RAP length and diameter change, variations of the RAP stiffness modulus, RAP elastic modulus and inflection stress, as a function of the slenderness ratio, show a linear function, which has an ascending trend when the slenderness ratio increases.
- When RAP diameter and length are changed, variations of the load ratio (tip to top) and settlement ratio (tip to top) at the design limit, as a function of slenderness ratio, make for an exponential function, which decreases with an increase in the slenderness ratio.
- The load ratio (tip to top) at the design limit, for the RAP with a diameter of 105 mm and bulging deformation, is about 5%, and in other RAPs with tip deformation, it is between 10% and 36%.
- The settlement ratio (tip to top) at the design limit, for the RAP with the diameter of 105 mm and bulging deformation, is about 14%, and in other RAPs with tip deformation, between 21% and 90%.
- When the length and diameter of RAPs are changed, increasing the applied stress at the top of the RAP raises the load ratio (tip to top) and decreases the RAP stiffness modulus.
- In field research and for testing RAPs, use of a cart-and-rail system can be a fast and economical method.
- The performance of the constructed dial settlement set was desirable for measuring the tip settlement of the small-scale RAPs. The use of this set is encouraged in real scale RAPs.
- In modulus load tests, by using the loading system designed for this study instead of reading three components of the settlement at the level of loading, it is possible to read one component of the settlement only. The designed loading system could also be used in plate load tests.

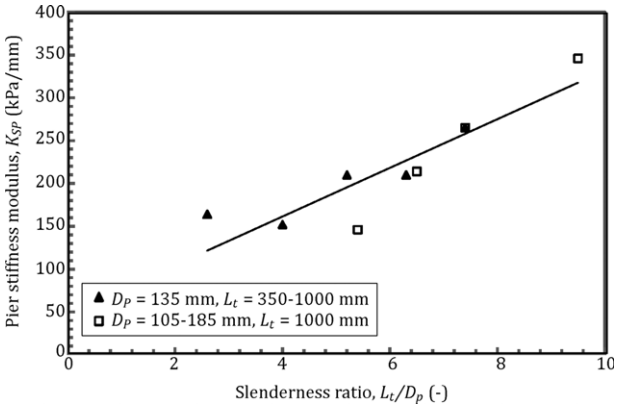

Figure 15: Comparison of pier stiffness modulus variations at design limit as a function of the slenderness ratio of RAPs.

- In this study, significant relationships were obtained between design limit parameters and slenderness ratios of different RAPs when changing the RAPs length and diameter. There has been less attention paid to this subject by other researchers, so far. Therefore, due to the possibility of obtaining design limit parameters as a function of the slenderness ratio in different areas, further research for finding similar relationships is encouraged.

Acknowledgments

This research was sponsored by the Transportation Research Institute of the Iranian Ministry of Road & Transportation (under Contract No. 86B1P1P23(GEO)). The authors of this paper are also grateful for the valued support of the Construction Deputy Governor General of the Province of Bushehr and the Director of the Bushehr Special Economic Zone.

References

[1] Lawton, E.C., Fox, N.S. and Handy, R.L. "Control of settlement and uplift structures using short aggregate piers", *Proceeding of the In-Situ Deep Soil Improvement*, Geotechnical Special Publication No. 45, ASCE, Atlanta, pp. 121–132 (1994).
[2] Lawton, E.C. and Fox, N.S. "Settlement of structures supported on marginal or inadequate soils stiffened with short aggregate piers", *Vertical and Horizontal Deformations of Foundations and Embankments*, ASCE Geotechnical Special Publication, 2 (40), pp. 962–974 (1994).
[3] Lawton, E.C. and Warner, B.J. "Performance of a group of geo-pier elements loaded in compression compared to single geo-pier elements and unreinforced soil", Final Rep., Rep. No. UUCVEEN 04-12, Univ. of Utah, Salt Lake City (2004).
[4] Wissmann, K.J., Moser, K. and Pando, M. "Reducing settlement risks in residual piedmont soil using rammed aggregate pier elements", *Proceeding of the Foundations and Ground Improvement*, Geotechnical Special Publication No. 113, ASCE, Blacksburg, Va., pp. 943–957 (2001).
[5] Wissmann, K.J., White, D.J. and Lawton, E. "Load test comparisons for rammed aggregate piers and pier groups", *Proceeding of the Geo Denver 2007 Congress*, Geotechnical Special Publication No. 172, ASCE, Denver (2007).
[6] Allgood, C., Weppler, L., Lien, B.H. and Fox, N.S. "Geo-pier intermediate foundation systems—case studies for building foundations over soft organic soils and peat", *Proceeding of the Nottingham Problematic Soils Conference* (2003).
[7] Farrell, T. and Taylor, A. "Rammed aggregate pier design and construction in California; performance, constructability, and economics", *Proceeding of the Structural Engineers Association of California 2004*, Placerville, CA (2004).
[8] White, D.J., Gaul, A.J. and Hoevelkamp, K. "Highway applications for rammed aggregate pier in Iowa soils", Final Rep., Iowa DOT TR-443, Ames, Iowa (2003).
[9] White, D.J., Pham, H.T.V. and Hoevelkamp, K.K. "Support mechanisms of rammed aggregate piers. I: experimental results", *J. Geotech. Geoenviron. Eng.*, 133(12), pp. 1503–1511 (2007).
[10] Handy, R.L. and White, D.J. "Stress zones near displacement piers. I: plastic and liquefied behavior", *J. Geotech. Geoenviron. Eng.*, 132(1), pp. 54–62 (2006).
[11] Handy, R.L. and White, D.J. "Stress zones near displacement piers. II: radial cracking and wedging", *J. Geotech. Geoenviron. Eng.*, 132(1), pp. 63–71 (2006).
[12] White, D.J. and Suleiman, M.T. "Design of short aggregate piers to support highway embankments", *Transportation Research Record, 1868*, Transportation Research Board, Washington, DC, pp. 103–112 (2005).
[13] White, D.J., Pham, H.T. and Wissmann, K.J. "Numerical simulation of construction-induced stresses around rammed aggregate piers", *Proceeding of the Int. Conf. on Numerical Simulation of Construction Processes in Geotechnical Engineering for Urban Environment*, NSC06, Bochum, Germany, pp. 257–264 (2006).
[14] Wissmann, K.J., Shields, C.S. and FitzPatrick, B.T. "Modulus load test results for rammed aggregate piers^{TM} in granular soils", *Geotechnical Special Publication*, (124), pp. 460–472 (2004).
[15] Suleiman, M.T. and White, D.J. "Load transfer in rammed aggregate piers", *Int. J. Geomech.*, 6(6), pp. 389–398 (2006).
[16] Randolph, M.F. and Wroth, C.P. "Analysis of deformation of vertically loaded piles", *ASCE J. Getech. Eng. Div.*, 104(12), pp. 1465–1488 (1978).
[17] Wissmann, K., Fox, N.S. and Martin, J.P. "Rammed aggregate piers defeat 75-feet long driven piles", *Proceeding of the Performance Confirmation of Constructed Geotechnical Facilities*, ASCE Special Publication No. 194, Amherst, Mass., pp. 198–211 (2000).

Hamid Reza Rezeghi received his Ph.D. degree from Tohoku University, Japan, in 2000 and is now Assistant Professor in the School of Civil Engineering at Iran University of Science and Technology, in Iran. His research interests lie in geotechnical and geoenvironmental engineering.

Bahman Niroumand graduated in Civil Engineering (B.S. degree) from Isfahan University of Technology, Isfahan, Iran, in 1992, and received his M.S. degree in Geotechnical Engineering from Tarbiat Modarres University, Tehran, Iran, in 1996. He is currently Faculty Member of the Persian Gulf University and a Ph.D. researcher at Iran University of Science and Technology, where he is studying Geotechnical Engineering. His research interests include experimental investigations on short rammed aggregate piers, slope stability, soil reinforcement and stabilization. He has published several papers and books.

Hossein Ghiassian is Associate Professor of Geotechnical Engineering in the School of Civil Engineering at Iran University of Science and Technology. He received his Ph.D. degree from the University of Michigan, Ann Arbor, USA, in 1995. Dr. Ghiassian's research interests mainly cover soil improvement, reinforcement and stabilization, slope stability and excavations, and also coastal geotechnique and protective systems. He has published and presented numerous technical papers in journals and at conferences.